Modal properties and thermal behaviors of high quality factor quasi-photonic crystal microcavity with different central post sizes

Tsan-Wen Lu*, Po-Tsung Lee, Chung-Chuan Tseng, and Yi-Yu Tsai

Department of Photonics and Institute of Electro-Optical Engineering, National Chiao Tung University
Rm. 415, CPT Building, 1001 Ta Hsueh Road, 300 Hsinchu, Taiwan, R.O.C.

ricky.eo94g@nctu.edu.tw

Abstract: We investigate the variations of modal properties of 12-fold quasi-photonic crystal microcavities sustaining whispering-gallery (WG) mode with different central post sizes both in simulations and experiments. We realize our design by a series of dry- and wet-etching processes. WG mode lasing actions are obtained with high quality (Q) factor of 8,400 from microcavity with effective post size 420 nm in diameter. Loss and thermal behaviors are analyzed by measured Q factors, thresholds, and rolling-off effects from light-in light-out curves of microcavities with increased post size. By finite-element simulations, we also address the heat sink improvement due to presence of larger central post that is observed in measurements.

OCIS codes: (050.5298) Photonic crystals; (140.5960) Semiconductor lasers; (140.3945) Microcavities

References and links

1. O. Painter, P. K. Lee, A. Scherer, A. Yariv, J. D. O'Brien, P. D. Dapkus, and I. Kim, "Two-Dimensional Photonic Band-Gap Defect Mode Laser," Science **284**, 1819-1821 (1999).
2. H. G. Park, J. K. Hwang, J. Huh, H. Y. Ryu, S. K. Kim, J. S. Kim, and Y. H. Lee, "Characteristics of Modified Single-Defect Two-Dimensional Photonic Crystal Lasers," IEEE J. Quantum Electron. **38**, 1353-1365 (2002).
3. Y. Akahane, T. Asano, B. S. Song, and S. Noda, "High-Q photonic nanocavity in a two-dimensional photonic crystal," Nature (London) **425**, 944-947 (2003).
4. K. Nozaki, S. Kita, and T. Baba, "Room temperature continuous wave operation and controlled spontaneous emission in ultrasmall photonic crystal nanolaser," Opt. Express **15**, 7506-7514 (2007).
5. H. Y. Ryu, M. Notomi, G. H. Kim, and Y. H. Lee, "High quality-factor whispering-gallery mode in the photonic crystal hexagonal disk cavity," Opt. Express **12**, 1708-1719 (2004).
6. H. G. Park, S. K. Kim, S. H. Kwon, G. H. Kim, S. H. Kim, H. Y. Ryu, S. B. Kim, and Y. H. Lee, "Single-Mode Operation of Two-Dimensional Photonic Crystal Laser With Central Post," IEEE Photon. Technol. Lett. **15**, 1327-1329 (2003).
7. S. L. McCall, A. F. J. Levi, R. E. Slusher, S. L. Pearton, and R. A. Logan, "Whispering gallery mode microdisk lasers," Appl. Phys. Lett. **60**, 289-291 (1992).
8. T. Baba, M. Fujita, A. Sakai, M. Kihara, and R. Watanabe, "Lasing characteristics of GaInAsP-InP strained quantum-well microdisk injection lasers with diameter of 2-10 μm," IEEE Photon. Technol. Lett. **9**, 878-880 (1997).
9. H. G. Park, S. H. Kim, S. H. Kwon, Y. G. Ju, J. K. Yang, J. H. Baek, S. B. Kim, and Y. H. Lee, "Electrically Driven Single-Cell Photonic Crystal Laser," Science **305**, 1444-1447 (2004).
10. M. K. Seo, K. Y. Jeong, J. K. Yang, Y. H. Lee, H. G. Park, and S. B. Kim, "Low threshold current single-cell hexapole mode photonic crystal laser," Appl. Phys. Lett. **90**, 171122 (2007).
11. P. T. Lee, T. W. Lu, and F. M. Tsai, "Octagonal Quasi-Photonic Crystal Single-Defect Microcavity With Whispering Gallery Mode and Condensed Device Size," IEEE Photon. Technol. Lett. **19**, 710-712 (2007).
12. P. T. Lee, T. W. Lu, F. M. Tsai, and T. C. Lu, "Investigation of whispering-gallery mode dependence on cavity geometry in quasiperiodic photonic crystal microcavity lasers," Appl. Phys. Lett. **89**, 231111 (2006).
13. S. K. Kim, J. H. Lee, S. H. Kim, I. K. Hwang, Y. H. Lee, and S. B Kim, "Photonic quasicrystal single-cell cavity mode," Appl. Phys. Lett. **86**, 031101 (2005).
14. K. Nozaki and T. Baba, "Quasiperiodic photonic crystal microcavity lasers," Appl. Phys. Lett. **84**, 4875-4877 (2004).

#97285 - $15.00 USD Received 10 Jun 2008; revised 29 Jul 2008; accepted 31 Jul 2008; published 5 Aug 2008

15. M. E. Zoorob, M. D. B. Charlton, G. J. Parker, J. J. Baumberg, and M. C. Netti, "Complete photonic bahdgaps in 12-fold symmetric quasicrystals," Nature (London) **404**, 740-743 (2000).
16. K. Nozaki, A. Nakagawa, D. Sano, and T. Baba, "Ultralow Threshold and Single-Mode Lasing in Microgear Lasers and Its Fusion With Quasi-Periodic Photonic Crystals," IEEE J. Sel. Topics Quantum. Electron. **9**, 1355-1360 (2003).
17. J. R. Cao, P. T. Lee, S. J. Choi, R. Shafiiha, S. J. Choi, J. D. O'Brien, and P. D. Dapkus, "Nanofabrication of photonic crystal membrane lasers," J. Vac. Soc. Technol. B **20**, 618-621 (2002).
18. O. Painter and K. Srinivansan, "Polarization properties of dipolelike defect modes in photonic crystal microcavities," Opt. Lett. **27**, 339-341 (2002).
19. P. T. Lee, T. W. Lu, F. M. Tsai, and T. C. Lu, "Investigation of whispering gallery mode dependence on geometry of quasiperiodic photonic crystal microcavity lasers," Appl. Phys. Lett. **89**, 231111 (2006).
20. P. T. Lee, J. R. Cao, S. J. Choi, Z. J. Wei, J. D. O'Brien, and P. D. Dapkus, "Operation of photonic crystal membrane lasers above room temperature," Appl. Phys. Lett. **81**, 3311-3313 (2002).
21. J. Limpert, T. Schreiber, A. Liem, S. Nolte, H. Zellmer, T. Peschel, V. Guyenot, and A. Tünnermann, "Thermo-optical properties of air-clad photonic crystal fiber lasers in high power operation," Opt. Express **11**, 2982-2990 (2003).

1. Introduction

Since the first demonstration of photonic crystal microcavity laser in 1999 by O. Painter *et al*. [1], various photonic crystal (PC) microcavities have been proposed and demonstrated [2-5]. However, most of them are operated under optical pumping. In order to promote this kind of device to practical applications in various systems, including advanced optical communications, photonic integrated circuits, biological sensors, and so on, searching a proper electrical-driven structure becomes necessary and important. From past related researches, the concept of inserting a central post under the microcavity [2, 5-6] originated from micro-disks [7, 8] has been regarded as a promising solution. For resonance modes with central zero field distributions, for example, whispering-gallery (WG) mode, the inserted central post can be efficiently served as a current injection pathway with relatively slight influences on the lasing performance. Furthermore, the post also plays the roles of side mode reducer and heat sinker. The first demonstration of electrically-driven PC microcavity laser with monopole mode using the central post structure is achieved by H. G. Park *et al*. [9]. Their results showed threshold of 250 μA and quality (*Q*) factor of 3,500 when the post size is 0.64 times lattice constant (*a*) in diameter. However, compared with monopole mode, it is no doubt that the WG mode with large central zero-field distribution will be more suitable for this structure. Very recently, the electrically-driven lasing actions of WG (hexapole) mode using the same structure are also achieved and reported by the same group [10]. Even so, adding a central post under the microcavity without affecting the lasing mode is still very crucial and can be further improved both in structure design and fabrication tolerances. Besides, the thermal properties when inserting a central post should be also investigated towards continuous-wave-driven PC nano and microcavity lasers. Here the in-plane confinement mechanism of WG mode in photonic crystal microcavity is actually different from that in microdisk. The former is due to the photonic bandgap effect and the latter is due to total internal reflection. But for convenience we also call this resonance mode as WG mode Because of its similar mode profile.

In our previous works, we have made lots efforts on microcavities formed by various non-periodic quasi-photonic crystals (QPCs). Based on these kinds of QPC microcavities, WG modes with different azimuthal numbers and high *Q* factors can be well sustained, which have been investigated and identified both in simulations and experiments [11, 12]. In this report, we adopt the 12-fold QPC [13] D_2 microcavity [12, 14-15] design formed by removing seven central air holes due to its sustained high *Q* WG mode and further investigate the WG modal properties in experiments and simulations when inserting the central post under the microcavity. Although the cavity size in our design is larger than that of single-defect microcavity, the central post fabrication tolerance and heat sink effect would be larger and better than those of single-defect microcavity. Also, lower turn-on voltage than the previous report [9] due to lower electrical resistance in electrical-driven structure could also be

#97285 - $15.00 USD Received 10 Jun 2008; revised 29 Jul 2008; accepted 31 Jul 2008; published 5 Aug 2008

expected. Based on above proposal, we fabricate 12-fold QPC D_2 microcavities with central posts and various post sizes by well controlling the wet-etching time. The basic WG modal and loss behaviors due to the inserted central posts are investigated by three-dimensional (3D) finite-difference time-domain (FDTD) method. From the well-fabricated devices, we also compare the measured lasing characteristics of microcavities with and without the central post, including their *Q* factors, thresholds, and thermal effects. Furthermore, we also simulate the heat sink improvement due to the presence of larger central post by finite-element method (FEM). And according to these results, the trade-off between the *Q* factor and thermal improvement when designing the central post size is also discussed and addressed.

2. Design and Simulation

The scheme of 12-fold QPC microcavity with central post is shown in Fig. 1(a). The QPC patterns are defined by air holes on a thin dielectric slab with 220 nm thickness and refractive index of 3.4. At first, we calculate the resonance modes in this microcavity without the central post by 3D FDTD method. The relationship between hole radius (*r*) over *a* ratio (*r/a* ratio) and normalized frequencies of defect modes in the photonic band-gap (PBG) region is shown in Fig. 1(b). The corresponding mode profiles in magnetic field are also shown in the figure and the potential candidates of resonance modes for the microcavity with central post are the first order WG modes with azimuthal numbers four, five, six, and seven, which are denoted by $WG_{4,1}$, $WG_{5,1}$, $WG_{6,1}$, and $WG_{7,1}$, respectively. The former sub-number denotes the azimuthal number and the latter one denotes the order of radial mode. In addition, the *Q* factor of each defect mode in the microcavity evaluated from energy decay curve is also shown in Fig. 1(b). We obtain high *Q* factor of 38,000 from $WG_{6,1}$ mode, and its effective mode

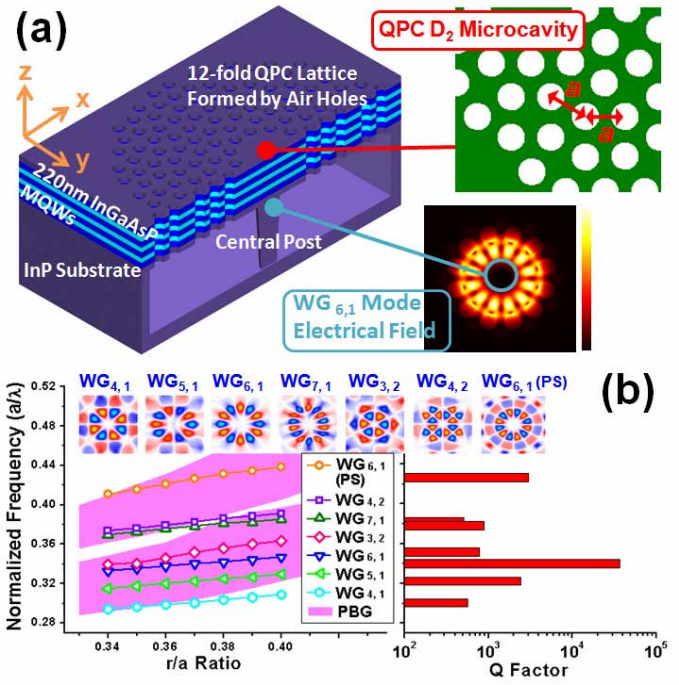

Fig. 1: (a) Scheme of 12-fold QPC D_2 microcavity with the central post. The microcavity design and the $WG_{6,1}$ mode profile in electrical field with significant zero-field distribution region are also shown in the insets. (b) (Left) The plot of simulated defect mode frequency versus *r/a* ratio. The PS denotes the phase-shifting mode [16]. (Top) The mode profile in magnetic field and (Right) simulated *Q* factor of each defect mode. The highest *Q* factor of 38,000 from $WG_{6,1}$ mode is obtained.

#97285 - $15.00 USD Received 10 Jun 2008; revised 29 Jul 2008; accepted 31 Jul 2008; published 5 Aug 2008

volume is calculated to be 1.6 $(\lambda/n)^3$. This is not surprising due to the enhancement of $WG_{6,1}$ mode from micro-gear effect [16] and indicates that $WG_{6,1}$ mode will be the dominant mode. Besides, we further investigate the degraded resonance behavior due to the perturbation caused by the inserted central post. The plot of simulated *Q* factor and wavelength of $WG_{6,1}$ mode versus post size in diameter is shown in Fig. 2(a). In the beginning, the *Q* value shows very little variation with the increased post size. However, when the post size is larger than 1.6*a* in diameter, the *Q* factor degrades dramatically. To further understand this phenomenon, the electrical-field distributions in *x*-*z* plane are shown in the inset of Fig. 2(a). There is no significant leaky energy flow through the post observed when the post size is 0.8*a* in diameter. However, when the post size increases to 2.4*a* in diameter, the WG mode is destroyed by the significant leaky energy flow through the post, which corresponds for the degradation of *Q* factor. Also, from the Fourier-transformed electrical fields in *x*-*y* plane shown in Fig. 2(b), we can observe the significant extra leaky components inside the light cone (black circle) induced by the larger post size of 2.4*a* in diameter when compared with that of 0.8*a* in diameter. Nevertheless, from the simulated results, we can still conclude that there would be only very slight influences on the WG mode lasing performance when the post size is smaller than 1.6*a* in diameter, which shows the advantage of employing WG mode and indicates large design and fabrication tolerances.

3. Fabrication

The QPC patterns are defined and fabricated on an epitaxial structure consisting of four 10 nm 1.2 % compressively-strained InGaAsP multi-quantum-wells (MQWs) by electron-beam lithography and a series of inductively coupled plasma / reactive-ion etching dry-etching process. And then the membrane structure is formed by HCl : H_2O = 3 : 1 selective wet-etching process. During this process, in order to obtain more precise control of post formation, the solution temperature is fixed at 2 °C to slow down the etching rate, which is estimated to be 1.05 μm / min along <-1, 0, 0> direction of InP [17]. By fine tuning the dipping duration from 80 to 110 seconds by 5 seconds per step, we obtain InP central posts with different post sizes from 1.4 to 0.2 μm in diameter. We also design some dummy patterns surround the QPC pattern to make sure that the post will be formed under the center of the microcavity [9]. Scanning electron microscope (SEM) pictures of the fabricated devices are shown in Fig. 3(a) and (b). In the following measurements and analysis, in order to fairly evaluate the perturbations caused by the central posts, we define and use the effective post size in diameter (*D*) instead of the real post size. The effective post size in radius is defined as the distance from the cavity center to the outermost position occupied by the post. Both the effective and

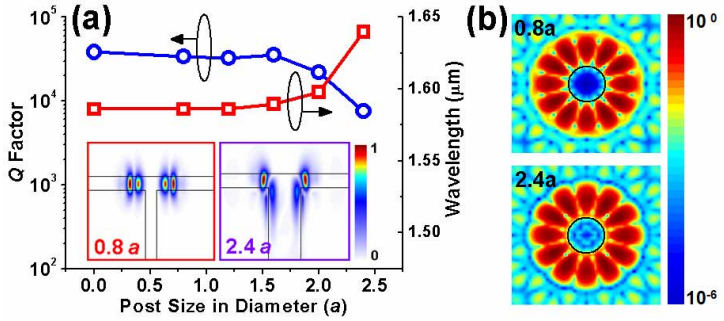

Fig. 2: (a) The relationship between the central post diameter and *Q* factor and wavelength of $WG_{6,1}$ mode. The *Q* factor dramatically degrades when the post size is larger than 1.6*a* in diameter. The insets indicate the energy flows in *x*-*z* plane. (b) Fourier-transformed electric fields in *x*-*y* plane when the central post sizes are 0.8*a* and 2.4*a*, which show the extra leaky components induced by larger central post.

#97285 - $15.00 USD Received 10 Jun 2008; revised 29 Jul 2008; accepted 31 Jul 2008; published 5 Aug 2008

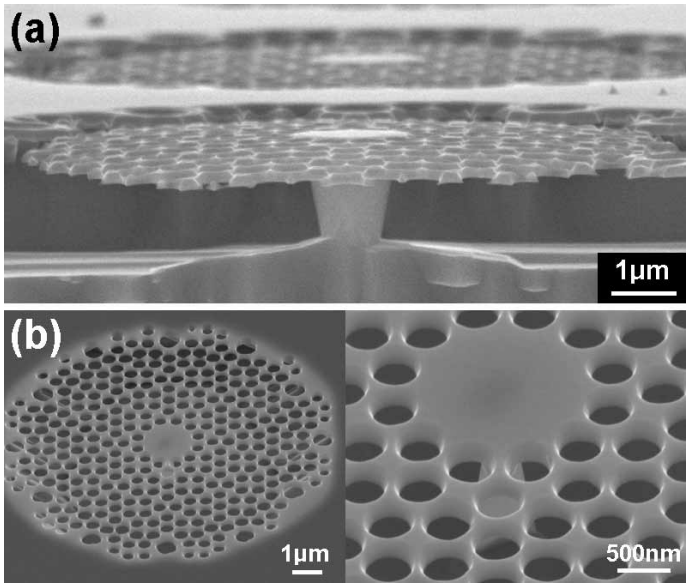

Fig. 3: (a) Cross-section SEM picture of 12-fold QPC D_2 microcavity supported by a central post with around 1.4 μm in diameter. (b) Tilted-view SEM pictures of 12-fold QPC D_2 microcavity with a D = 420 nm central post.

real post sizes are directly estimated from the side-view SEM pictures and the shadow caused by electron accumulation from the top-view SEM pictures.

4. Measured Modal and Thermal Characteristics

Under pulsed-pumping at room temperature by an 845 nm diode laser with 25 ns pulse width, 0.5 % duty cycle, and 2.5 μm spot size in diameter, we obtain lasing actions from 12-fold QPC D_2 microcavities with various sizes of central posts from the spectrometer with 0.05 nm resolution. Their measured light-in light-out (*L-L*) curves and lasing spectra above and near thresholds are shown in Fig. 4 and Fig. 5(a). Comparing the lasing properties of microcavities without central post and with post size D = 420 nm, their thresholds are both estimated as 0.35 mW from L-L curves and the measured Q factor slightly degrades from 9,300 to 8,400 in Fig. 5(a). Their lasing wavelengths are 1582.2 and 1589.5 nm, respectively. Besides, we also obtain WG mode lasing action from the microcavity with a smaller post size of D = 200 nm and with Q ~ 9,000, which is almost the same as that of the microcavity without central post. Thus, all of these indicate the small influence on the WG mode lasing due to the presence of central post with D smaller than 420 nm (~ 0.76a). On the other hand, when D increases to 900 nm (~ 1.65a), the threshold increases to 1.2 mW and the Q factor degrades to 6,300. Finally, when D further increases to be larger than 900 nm, no $WG_{6,1}$ mode lasing is observed anymore. These measured results also quite agree with the trend of our simulated results presented in Fig. 2. Besides, when the post size comes close to the cavity size, in our case, 1.2 to 1.4 μm in diameter, the microcavity becomes an asymmetric structure. In this case, we observe low Q $WG_{3,2}$ mode lasing actions instead of $WG_{6,1}$ mode at wavelengths from 1400 to 1450 nm with high thresholds of 3.2 to 5 mW and low measured Q factors of 2,500 to 3,000.

In Fig. 5(b), the measured WG mode polarizations show low polarized ratios (defined as maximum over minimum collected power) of 2.2 and 1.5 before and after inserting the central post. Although the polarized direction is changed after inserting the central post, the little variation in polarized ratio still indicates slight influence on WG mode caused by the inserted central post. Besides, these low polarized ratios also indicate the uniformity of our fabrication process due to the low symmetry breaking [10, 18]. In fact, the ideal WG mode in the

#97285 - $15.00 USD Received 10 Jun 2008; revised 29 Jul 2008; accepted 31 Jul 2008; published 5 Aug 2008

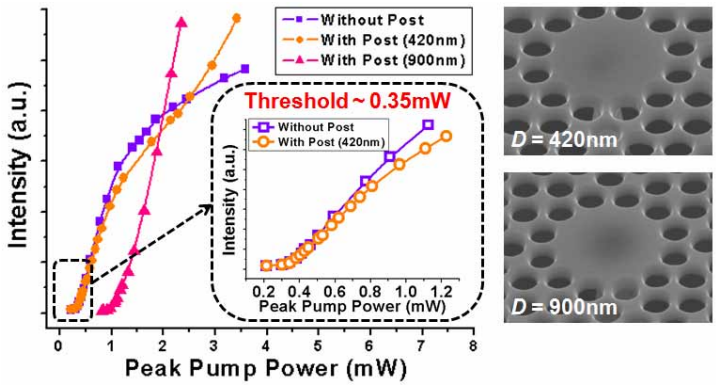

Fig. 4: *L-L* curves of 12-fold QPC D_2 microcavities without and with central posts when D = 420 and 900 nm. The thresholds are estimated to be 0.35, 0.35, and 1.2 mW, respectively. SEM pictures of microcavities with different post sizes are also shown.

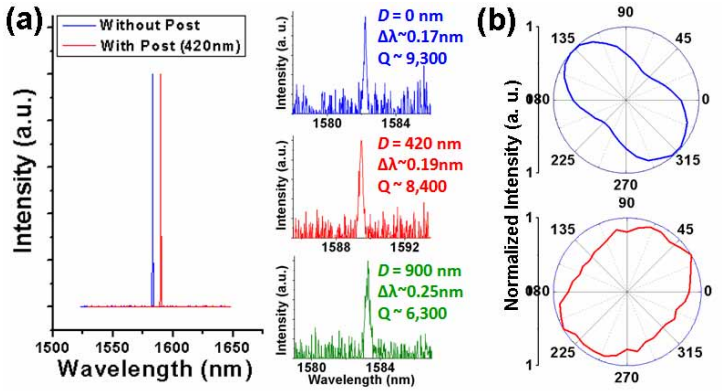

Fig. 5: (a) Lasing spectra above and below (~ 0.8 times) thresholds. The measured Q factor decreases from 9,300 to 6,300 when D increases from 0 to 900 nm. (b) The angular plots show the measured WG mode polarizations before (top) and after (bottom) inserting the central post with low polarized ratios of 2.2 and 1.5.

photonic crystal microcavity is un-polarized (i.e. polarized ratio is equal to 1) due to its well balanced inner symmetry of the mode and the cavity boundary (nearest air holes). However, in real case, this symmetry can be easily destroyed by perturbations, mainly from fabrication imperfections of nearest air holes [19]. Thus, the WG mode will become polarized and the polarization degree (polarized ratio) will increase with the perturbations. Thus, small polarization degree indicates less fabrication imperfection and better uniformity of fabricated air holes of the sample.

It is also worthy to mention the observed rolling-off phenomenon under increased pump power level with different post sizes. From the *L-L* curves in Fig. 4, the fast rolling-off due to poor heat dissipation of the membrane structure is observed. In contrast, it is significantly improved when inserting the post with D = 420 nm. When D further increases to 900 nm, the rolling-off effect disappears under the similar pump level and implies the improvement of heat sink. To further confirm this measured improvement due to the presence of central post, we simulate the thermal behaviors of 12-fold QPC D_2 microcavity with and without the central post by FEM. The simulation setup and scheme of 12-fold QPC D_2 microcavity membrane structure formed by Air / InGaAsP / Air is illustrated in Fig. 6(a). The QPC lattice constant, r/a ratio, and membrane thickness are set to be 550 nm, 0.38, and 220 nm, respectively. To

#97285 - $15.00 USD Received 10 Jun 2008; revised 29 Jul 2008; accepted 31 Jul 2008; published 5 Aug 2008

accelerate our simulation, we reduce the simulation domain to be one-sixth of the whole structure due to the lattice symmetry feature. The initial temperature of the simulation domain is 300 K and the boundaries are set to be axial symmetric [20]. Besides, during the simulations, we also find that the contributions of heat radiation and convection are relative low compared with that of heat conduction, that is, the conduction dominates the heat transfer behavior [21]. The conductive heat transfer model is given by:

$$\rho \times C \frac{\partial T}{\partial t} + \nabla \cdot (-k \nabla T) = H$$

where ρ, k, and C represent the density, thermal conductivity, and thermal capacity of material, respectively. The H denotes a time- and position-dependent surface heat source we give in the simulation, which is an exponential decay form related to the absorption coefficient α (~ 3.5×10^6) of InGaAsP material. Referred to our measurement conditions, the pulse width, duty cycle, energy level, and pump area of H are set to be 25 ns, 0.5 %, 2 mW, and 1 μm in radius, respectively. Coefficients for different materials used in the simulation are listed in Table. I. The simulated temperature distribution of 12-fold QPC D_2 microcavity membrane structure is shown in Fig. 6(b). The highest temperature occurs at the central region with a 12.3 K increase above room temperature (300 K), which is a reasonable value under pulse excitation. And then, we further insert different central posts with sizes of 440, 660, and 880 nm in diameter under the microcavity. The simulated results are also shown in Fig. 6(b) and the highest temperatures are 310.2, 308.9, and 307.7 K, respectively. In addition, we also calculate the temperature decay time at the region where WG mode most concentrates by first

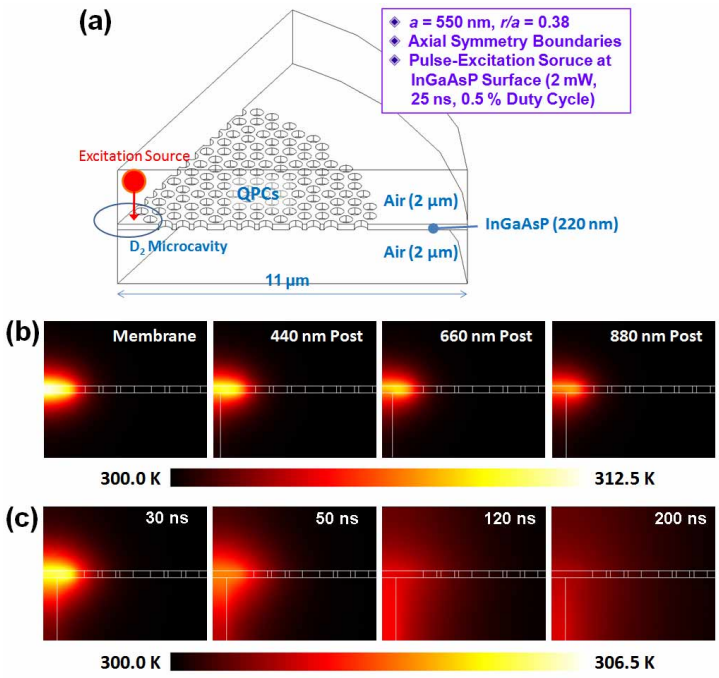

Fig. 6: (a) The scheme of the 12-fold QPC D_2 microcavity for FEM simulation. (b) The simulated temperature distributions of microcavities without and with central post sizes of 440, 660, and 880 nm in diameter. The temperature is decreased when the post size is increased. (c) The simulated temperature distributions of microcavity with central post size of 880 nm in diameter when the time is 30, 50, 120, and 200 ns. The heat flow is mainly through the central post.

#97285 - $15.00 USD Received 10 Jun 2008; revised 29 Jul 2008; accepted 31 Jul 2008; published 5 Aug 2008

Table. I: Coefficients for different materials used in heat transfer simulation (in M.K.S. unit).

Material	ρ (kg / m^3)	C (J / kg.K)	k (W / m.K)
Air	1.205	1006	0.025
InP	4810	310	68
InGaAsP	5445.2	282.3	39.9

order exponential fitting from the transient solutions. The decay time is defined as the time duration for the temperature drop to *1/e* of its highest value. The results obtained are 53.8, 42.0, 37.0, and 31.5 ns, which show the faster heat dissipation due to the presence of larger central post. To further understand the extra heat sink provided by the post, the temperature distribution of microcavity with 880 nm central post at different times of 30, 50, 120, and 200 ns are shown in Fig. 6(c). In Fig. 6(c), the heat flow (dissipation) is mainly through the central post from t = 30 to 200 ns, which is a direct evidence of thermal improvement due to presence of the central post. Although these experimental and simulation results strongly indicate the better heat sinking property of the microcavity with larger central post, one should still carefully analyze and deal with the trade-off between Q factor degradation and heat sinking. One can enlarge the central post to improve heat dissipation, but on the other hand the microcavity design has to be re-optimized to maintain its high Q resonance mode. And then the continuous-wave electrically-driven PC microcavity laser could be expected.

5. Conclusion

In summary, we investigate the resonance behaviors of 12-fold QPC D_2 microcavity by 3D FDTD method. High simulated Q factor of 38,000 from $WG_{6,1}$ mode with significant zero-field distribution region is obtained, which can be a good mode candidate for microcavity with central post. By investigating Q factor degradation of $WG_{6,1}$ mode under different post sizes, we can conclude that there would be only slight influence on WG modal properties when the post size is smaller than 1.6a in diameter. By well-controlled wet-etching process and proper pattern design, we fabricate microcavities with various central post sizes. In measurements, the WG mode lasing action is obtained from microcavity with D = 420 nm and with high measured Q factor of 8,400 and threshold of 0.35 mW, same as that of microcavity without central post. We also obtain lasing actions with higher threshold of 1.2 mW and lower Q factor of 6,300 when D is as large as 900 nm. When the post size increases, improved rolling-off effect from L-L curves and degraded Q factors are both observed. To further prove the heat sink improvement provided by the central post, we apply FEM simulation. Comparing the simulated results of membrane microcavity and microcavity with 880 nm central post, the highest temperature is decreased from 312.3 to 307.7 K and the decay time is reduced from 53.8 to 31.5 ns. From these results, we also conclude that there will be trade-off between Q factor and improved heat sink effect when designing the central post size. We believe this microcavity with central post based on $WG_{6,1}$ mode is very promising under the requirements of large design and fabrication tolerances to achieve electrically-injected QPC microcavity laser with low threshold, high Q factor, and improved thermal effect.

Acknowledgements

This work is supported by Taiwan's National Science Council (NSC) under contract numbers NSC-96-2120-M-009-010 and NSC-95-2221-E-009-056-MY3. The authors would like to thank the help from Center for Nano Science and Technology (CNST) of National Chiao-Tung University, Taiwan.

#97285 - $15.00 USD Received 10 Jun 2008; revised 29 Jul 2008; accepted 31 Jul 2008; published 5 Aug 2008